Vibronic transition probabilities in the excitation spectra of the Pr^{3+} ion

1992 J. Phys.: Condens. Matter 4 8889

(http://iopscience.iop.org/0953-8984/4/45/021)

J. Phys.: Condens. Matter 4 (1992) 8889–8902. Printed in the UK

Vibronic transition probabilities in the excitation spectra of the Pr^{3+} ion

C de Mello Donegá, A Meijerink and G Blasse

Debye Research Institute, University of Utrecht, PO Box 80000, 3508TA Utrecht, The Netherlands

Received 13 July 1992, in final form 17 September 1992

Abstract. Vibronic features are observed in the excitation spectrum of Pr^{3+} in several host lattices. Vibronic transition probabilities, A_{VIB}, for the $^3H_4 \rightarrow {}^3P_0$ excitation transition on Pr^{3+} are reported. A_{VIB} varies by two orders of magnitude from LaF_3 to Y_2O_2S. These observations are discussed in terms of existing theories of the intensity of vibronic transitions in the intraconfigurational $4f^n$ spectra. The observed variation can be qualitatively accounted for by the differences in covalency, polarizability and opposite-parity configuration admixing.

1. Introduction

The optical spectra of compounds containing trivalent rare-earth (RE) ions often show weak vibronic features. The intensity of vibronic transitions is determined by the strength of the electron–lattice coupling. Consequently, the relative intensities of the vibronic lines are of special interest as diagnostic probes for the RE–Ligand interactions and crystal-field dynamics.

In order to understand the nature of such a coupling, our group has been investigating the vibronic transitions in the optical spectra of several rare-earth ions (Gd^{3+} [1], Eu^{2+} [2], Eu^{3+} [3], Pr^{3+} [4]). The intensity of the vibronic features depends strongly on the host lattice. Recently Blasse [5] has given an overview of the studies on vibronic transitions in the rare-earth ions.

The Pr^{3+} ion vibronics are worthwhile to investigate further. Intense vibronic sidebands were observed in Pr^{3+} for electronic transitions characterized by $\Delta J = 2$ and 4 [4]. The latter case is particularly interesting since it violates the selection rule which arises from the theoretical approaches to vibronic line intensity on rare-earth ions [6–9].

In this paper we report on the vibronic transition probabilities A_{VIB} for the $^3H_4 \rightarrow {}^3P_0$ excitation transition of the Pr^{3+} ion in several lattices at 4.2 K. A_{VIB} was observed to vary by two orders of magnitude. This host lattice dependence of A_{VIB} is discussed in terms of theories of the intensity of vibronic transitions in the intraconfigurational $4f^n$ spectra [6–9]. In addition we make a comparison with the vibronic transition probabilities of Gd^{3+} [1].

0953-8984/92/458889+14$07.50

2. Experimental details

All samples are powders and contain 1 mol% Pr^{3+} or less. The RE_2O_2S (RE = La, Y) samples were kindly supplied by Dr C W Struck. The remaining compositions investigated were prepared as described in the literature [4]. The samples were checked by x-ray powder diffraction analysis and found to be single phase. Diffuse reflectance spectroscopy showed that the samples do not contain Pr^{4+} or other optical impurities.

$LiYF_4$ has the inverse scheelite structure, space group $I4_1/a$ (C_{4h}^6). The Y^{3+} ion has S_4 site symmetry [10]. LaF_3 has the trigonal space group $P\bar{3}c1$ (D_{3d}^4), and C_2 site symmetry for the La^{3+} ions [11]. $Y_3Al_5O_{12}$ (YAG) has space group symmetry $Ia3d$ (O_h^{10}) and the Y^{3+} ions are in sites with D_2 symmetry [12]. LaOCl has the layered PbFCl structure, space group $P4/nmm$ (D_{4h}^7), and site symmetry C_{4v} for the La^{3+} ions [13]. La_2O_3 and RE_2O_2S are isostructural. They have $P\bar{3}m1$ (D_{3d}^3) space group symmetry and the site symmetry is C_{3v} for the RE^{3+} ions [14].

The low-resolution luminescence spectra were obtained by using a SPEX DM3000F Spectrofluorometer with double-grating 0.22 m SPEX 1680 monochromators and a 450 W Xe lamp. The instrument is equipped with an Oxford helium flow cryostat. The $4f^2 \rightarrow 4f5d$ excitation transition of Pr^{3+} in $LiYF_4$ was measured by using a Perkin–Elmer MPF-3L Spectrofluorometer with a deuterium lamp as excitation source.

High-resolution and decay measurements were performed on a set-up consisting of a LPD-3002 dye laser pumped by a LPX-100 excimer laser, equipped with an Oxford Instruments liquid helium cryostat. The emission monochromator is a SPEX 1704 (focal length 1 m). Spectra are obtained by measuring the photocurrent of the cooled photomultiplier tube (RCA C31034) by a Philips DC-micrometer PM 2436. For decay measurements the signal is sent to a Tektronix 2440 digital oscilloscope.

The Raman spectra of La_2O_3, La_2O_2S and Y_2O_2S were measured at the Inorganic Chemistry Laboratory of the University of Amsterdam. The sample is irradiated with an SP 171 Argon ion laser and the Raman spectrum is recorded with a Jobin–Yvon Ramanor HG2S spectrometer.

The infrared absorption spectra of La_2O_2S and Y_2O_2S were recorded between 200 cm^{-1} and 2000 cm^{-1} using a Perkin–Elmer 567 IR spectrometer and standard CsI pellet techniques.

3. Method and results

The energy level scheme of Pr^{3+} in LaF_3 [15] is shown in figure 1. Vibronic features were investigated for the intraconfigurational excitation spectrum ($^3H_4 \rightarrow {}^3P_{0,1,2}, {}^1I_6$) of the $^3P_0 \rightarrow {}^3H_6, {}^3F_2$ emission of Pr^{3+} ($4f^2$).

At 4 K the $^3H_4 \rightarrow {}^3P_0$ excitation transition consists of one electronic line at about 20 000 cm^{-1}, since the final level is non-degenerate and the lowest crystal-field component of the $^3H_4$ multiplet, i.e. $^3H_4^{(1)}$, is the only one significantly populated. This is a very suitable situation to observe vibronic lines. A comparable situation occurs for Gd^{3+} in emission [1]. However, in the case of Pr^{3+} there is a serious problem due to higher electronic levels. The $^3H_4^{(1)} \rightarrow {}^3P_1, {}^1I_6$ lines start at about 400 cm^{-1} higher energy. This imposes a limit on the observable vibronics. Consequently, the ratio R of the total integrated vibronic intensity and the zero-phonon line intensity

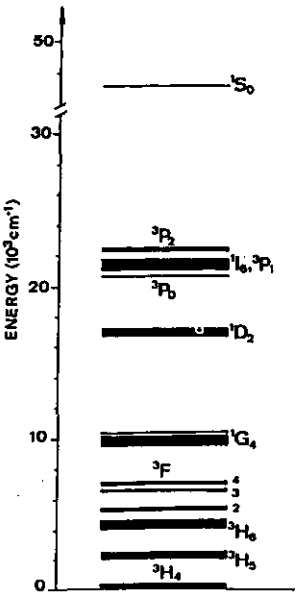

Figure 1. Energy level scheme of Pr^{3+} in LaF_3 (after [15]).

($R = I_{VIB}/I_{ZP}$) might be underestimated. The underestimation is assumed to be within 5–10% for all of the studied lattices except for $Y_3Al_5O_{12}$. In the last case the highest vibrational frequency is at about 900 cm^{-1} [16] and due to the crystal-field splitting, only vibronics up to 250 cm^{-1} can be considered. Therefore the underestimation of R in $Y_3Al_5O_{12}$ is expected to be significant.

The $^3H_4^{(1)} \rightarrow {}^3P_0$ excitation spectra of Pr^{3+} in the investigated compositions will be discussed below. As an example the vibronic part of the $^3H_4^{(1)} \rightarrow {}^3P_0$ spectrum of Pr^{3+} in $LiYF_4$ is shown in figure 2. Table 1 presents a comparison of the relative energy positions of the vibronic lines with the vibrational frequencies of $LiYF_4$. The agreement is seen to be good.

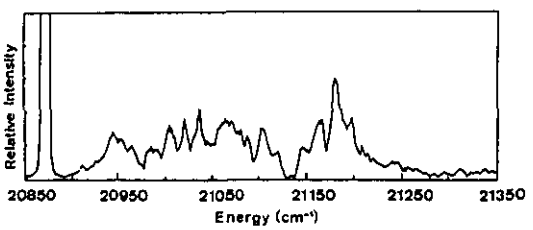

Figure 2. Vibronic part of the $^3H_4^{(1)} \rightarrow {}^3P_0$ excitation spectrum of the $^3P_0 \rightarrow {}^3H_6$ emission of Pr^{3+} in $LiYF_4$ at 4.2 K. The onset of the zero-phonon transition appears on the extreme left side of the spectrum.

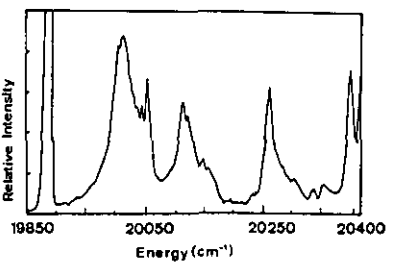

Figure 3. Vibronic part of the $^3H_4^{(1)} \rightarrow {}^3P_0$ excitation spectrum of the $^3P_0 \rightarrow {}^3F_2$ emission of Pr^{3+} in Y_2O_2S at 4.2 K. The onset of the zero-phonon transition appears on the extreme left side of the spectrum.

The zero-phonon line of the $^3H_4^{(1)} \rightarrow {}^3P_0$ transition of Pr^{3+} in Y_2O_2S is at 19 889 cm^{-1}. Vibronic lines are observed at 122, 158, 221, 248, 359, 393, 451 and

Table 1. Relative position of the vibronic lines in the $^3H_4^{(1)} \rightarrow {}^3P_0$ excitation spectrum of the $^3P_0 \rightarrow {}^3H_6$ emission of Pr^{3+} in $LiYF_4$ at 4.2 K. The zero-phonon line is at 20 873 cm^{-1}. All values are in cm^{-1}.

Vibronic position[a]	Vibrational frequency[b]
67	—
104	—
126	—
139	143(IR)
155	155(R)
180	177(R), 173(IR)
206	199(R), 195(IR)
219	224(IR)
238	248(R)
262	252(IR), 264(R)
281	283(IR)
297	303(IR)
315	329(R)
425	425(R), 424(IR)

[a] Relative to electronic origin.
[b] R = Raman, IR = Infrared, [17].

503 cm^{-1} from the zero-phonon line (figure 3). There is good agreement between these vibronic frequencies and those obtained from the vibronic side bands observed by Hoshina *et al* [18] in the $^7F_0 \rightarrow {}^5D_0$ and $^7F_0 \rightarrow {}^5D_1$ excitation transitions of Eu^{3+} in Y_2O_2S. The Raman spectrum of Y_2O_2S shows peaks at 144, 257, 443 and 473 cm^{-1}. The IR absorption spectrum (above 200 cm^{-1}) contains three bands with maxima at 220, 320 and 450 cm^{-1}. The latter is the most intense band and shows shoulders at 400 and 520 cm^{-1}.

In the $^3H_4^{(1)} \rightarrow {}^3P_0$ excitation spectrum of Pr^{3+} in La_2O_2S the zero-phonon line is observed at 20 046 cm^{-1}. The vibronic side band shows maxima at 120, 129, 179, 204, 230, 281, 311, 364, 389, 455 and 480 cm^{-1}. The Raman spectrum of La_2O_2S consists of lines at 107, 199, 363 and 395 cm^{-1}. The IR absorption spectrum shows maxima at 200, 315 and 400 cm^{-1}. The latter has a shoulder at 480 cm^{-1}. The immediate surroundings of the RE^{3+} ions are the same in both La_2O_2S and Y_2O_2S, since these lattices are isostructural. Therefore, the vibronic spectra of RE^{3+} ions are expected to be similar in both lattices. However, the vibronic intensity distribution and the relative position of the vibronic lines in La_2O_2S:Pr^{3+} are considerably different from those observed for Pr^{3+} in Y_2O_2S. Significant differences were also observed between the vibronic excitation spectra of Eu^{3+} in Y_2O_2S and in La_2O_2S [18]. These differences may be related to a large local lattice distortion for the substitution of Pr^{3+} or Eu^{3+} in Y_2O_2S, since the Y^{3+} sites are smaller than the substituting ions. A more detailed discussion of these observations would be desirable but lies beyond the scope of this paper.

In the excitation spectrum of $Y_3Al_5O_{12}$:Pr^{3+} the zero-phonon line of the $^3H_4^{(1)} \rightarrow {}^3P_0$ transition appears at 20 550 cm^{-1}. Vibronic features can be identified only up to 250 cm^{-1} from the electronic line. In this region maxima occur at 132 and 202 cm^{-1}. The IR absorption spectrum of $Y_3Al_5O_{12}$ shows maxima at 125, 181, 227, 298, 341, 403, 437, 505, 551, 590, 707, 769 and 921 cm^{-1} [16]. The Raman spectrum shows intense lines at 162, 218, 259, 340, 403, 408, 561, 719 and 783 cm^{-1} [16].

Figure 4 shows the vibronic part of the $^3H_4^{(1)} \rightarrow {}^3P_0$ excitation spectrum of Pr^{3+}

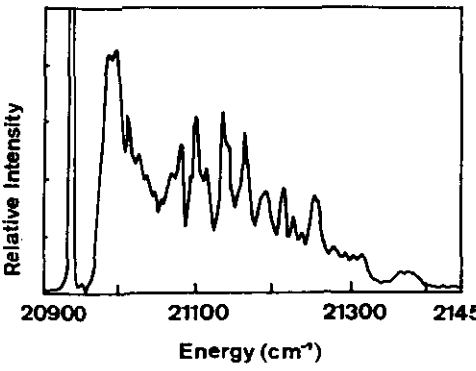

Figure 4. Vibronic part of the $^3H_4^{(1)} \rightarrow {}^3P_0$ excitation spectrum of the $^3P_0 \rightarrow {}^3H_6$ emission of Pr^{3+} in LaF_3 at 4.2 K. The onset of the zero-phonon transition appears on the extreme left side of the spectrum.

in LaF_3 at 4.2 K. The vibronic side bands agree well with those observed by Yen *et al* [19] in the absorption spectra of LaF_3:Pr^{3+} crystals at 4.2 K. The zero-phonon line is at 20 939 cm^{-1}. Vibronic lines are observed at 26, 47, 58, 73, 86, 101, 123, 138, 154, 170, 191, 217, 244, 270, 286, 313, 334, 345, 361, 372 and 425 cm^{-1} relative to the zero-phonon line. These frequencies agree with those obtained from the vibronic side bands of the $^6P_{7/2} \rightarrow {}^8S_{7/2}$ emission [1] and $^8S_{7/2} \rightarrow {}^6P_{7/2}^{(1)}$ excitation [20] transitions of Gd^{3+} in LaF_3 at 4.2 K. However, the vibronic intensity distribution in the Gd^{3+} spectra is different from that observed in the Pr^{3+} spectra (figure 4). The most intense vibronic lines in the Gd^{3+} spectra are observed at 179, 289, 318 and 362 cm^{-1} relative to the zero-phonon line [1, 20]. The IR absorption spectrum of LaF_3 at 70 K shows maxima at 106 (w), 130 (w), 170 (m), 219 (m), 261 (m), 281 (s), 350(s), 380 (s) and 420 (sh) cm^{-1} (w = weak, m = medium, s = strong, sh = shoulder) [21]. The polarized Raman spectra of LaF_3 crystals at 2.2 K show peaks at 78, 120, 146, 163, 203, 226, 230, 293, 301, 305, 314, 366 and 390 cm^{-1}, considering all orientations [22]. The acoustic vibrational modes of LaF_3:Pr^{3+} crystals at 1.8 K have been observed at 27.8, 29.5, 31.2, 33.0, 34.5, 43.3 and 51.9 cm^{-1} [23]. It seems that the strongest IR absorption bands appear as the strongest vibronic lines in the Gd^{3+} spectra, but not in the Pr^{3+} vibronic spectra.

The zero-phonon line of the $^3H_4^{(1)} \rightarrow {}^3P_0$ excitation transition of Pr^{3+} in La_2O_3 is at 20 280 cm^{-1}. The vibronic part of the spectrum shows maxima at 100, 116, 150, 203, 271, 310, 340, 388 and 419 cm^{-1} above the zero-phonon line. Most of the vibronic intensity is in the first four lines. Maxima in the IR absorption spectrum of Pr_2O_3 occur at 260, 385 and 450 cm^{-1} [14]. The Raman spectrum of La_2O_3 shows lines at 105, 190 and 407 cm^{-1}.

The excitation spectrum of LaOCl:Pr^{3+} in the $^3H_4^{(1)} \rightarrow {}^3P_0$ region shows vibronic features at 81, 107, 127, 174, 203 and 318 cm^{-1} from the the zero-phonon line at 20 282 cm^{-1}. The IR absorption spectrum of PrOCl shows four bands with maxima at 126, 193, 390 and 515 cm^{-1} [24, 25]. The Raman spectrum of PrOCl consists of five lines: 121, 185, 216, 346 and 458 cm^{-1} [25].

Most of the vibronic lines can be assigned to coupling with IR- and Raman-active vibrational modes, but it is not possible to assign all of the observed vibronic features. The vibronic coupling strength appears to be similar for Raman- and IR-active vibrations.

Now we turn to the transition probabilities for the vibronic transitions, which can be obtained from the ratio R, the decay time τ of the $^3P_0$ level and the fraction of

the $^3P_0 \rightarrow {}^3H_4^{(1)}$ emission in the total $^3P_0$ emission spectrum. It is assumed that the transition probabilities for the $^3H_4^{(1)} \leftrightarrow {}^3P_0$ transition are the same in absorption and emission. This is justified since the weak-coupling approximation applies. For the vibronic transitions of Gd^{3+} this has been verified experimentally [20]. Considering that

$$A_{RAD} = A_{VIB} + A_{ZP} \tag{1}$$

where A_{ZP} and A_{VIB} are the zero-phonon and the vibronic contributions to the total radiative transition probability A_{RAD}, the value of A_{VIB} can be derived from the following relation

$$R = I_{VIB}/I_{ZP} = A_{VIB}/A_{ZP}. \tag{2}$$

To calculate A_{VIB} in the $^3H_4^{(1)} \rightarrow {}^3P_0$ excitation transition at 4 K, A_{ZP} for the $^3P_0 \rightarrow {}^3H_4^{(1)}$ emission transition is obtained from the total transition probability of the $^3P_0$ level (A_{TOT}) and the relative integrated intensity of the $^3P_0 \rightarrow {}^3H_4^{(1)}$ emission line in the total $^3P_0$ emission spectrum at 4 K:

$$A_{ZP}/A_{TOT} = I_{(^3P_0 \rightarrow {}^3H_4^{(1)})}/I_{TOT}. \tag{3}$$

The total transition probability A_{TOT} is equal to τ^{-1}, since non-radiative decay processes can be neglected for two reasons [26]:

(i) multiphonon relaxation has a low probability, since the energy gap between the $^3P_0$ and $^1D_2$ levels is at least six times larger than the frequency of the available phonons;

(ii) energy-transfer or cross-relaxation processes are improbable in view of the low Pr^{3+} concentration.

The values of $I_{(^3P_0 \rightarrow {}^3H_4^{(1)})}$ and I_{TOT} are determined after correction of the emission spectra for the instrumental response and conversion to a photon flux per energy interval scale. The concentration of Pr^{3+} ions is 1 mol% in $Y_3Al_5O_{12}$, 0.5 mol% in LaF_3 and $LiYF_4$, and 0.1–0.05 mol% in the remaining lattices. These concentrations are low enough to prevent reabsorption of the $^3P_0 \rightarrow {}^3H_4^{(1)}$ emission in all samples except $Y_3Al_5O_{12}$. In the last case some reabsorption may occur, which will lead to an underestimation of A_{VIB}.

The estimated values of A_{VIB} for the $^3H_4^{(1)} \rightarrow {}^3P_0$ excitation transition and other relevant data are summarized in table 2. The position of the 4f5d configuration of the Pr^{3+} ion was estimated from the excitation spectra (maximum of the first $4f^2 \rightarrow 4f5d$ transition), except for LaF_3 [27]. The optical absorption edge of the studied lattices was estimated from the diffuse reflectance spectra, except for La_2O_3 [28], LaF_3 [29], $Y_3Al_5O_{12}$ [30] and $LiYF_4$. For $LiYF_4$ the position of the optical absorption edge is assumed to be similar to that of LaF_3.

Table 3 presents a comparison between the A_{VIB} values of the Gd^{3+} $^6P_{7/2} \rightarrow {}^8S_{7/2}$ emission transition [1] and the Pr^{3+} $^3H_4^{(1)} \rightarrow {}^3P_0$ excitation transition in the same host lattices. Since the emission and excitation vibronics of Gd^{3+} are known to be mirror images of each other, but the former are measured with more accuracy [20], the values of A_{VIB} were taken from the Gd^{3+} emission transition.

Table 2. Data on the Pr^{3+} $^3H_4^{(1)} \rightarrow {}^3P_0$ excitation transition in several compositions: investigated composition of the samples, integrated intensity ratios (R) of the vibronic part of the spectrum and the zero-phonon line, zero-phonon and vibronic transition probabilities (A_{ZP} and A_{VIB}) and the zero-phonon line position (ZP). The $^3P_0$ lifetime τ, the maximum of the first 4f5d excitation band and the optical absorption edge (OAE) of the lattice are also included. All measurements were performed at 4.2 K.

Sample	R	A_{ZP} (s^{-1})	A_{VIB} (s^{-1})	τ (μs)	Spectral position (cm^{-1})		
					ZP	4f5d	OAE
LaF_3:Pr	1.5	60	85	51	20 939	60 000	80 000
$LiYF_4$:Pr	0.12	840	100	48	20 873	50 000	80 000
$Y_3Al_5O_{12}$:Pr	0.1	3.0×10^3	300	11	20 550	35 000	45 000
LaOCl:Pr	0.4	2.1×10^3	900	7.3	20 282	40 000	44 000
La_2O_3:Pr	0.7	2.3×10^3	1600	3.6	20 280	35 000	44 000
La_2O_2S:Pr	0.7	1.6×10^4	11 000	3.0	20 046	33 000	42 000
Y_2O_2S:Pr	0.9	1.4×10^4	13 000	2.7	19 889	33 000	41 000

Table 3. A_{VIB} and A_{ZP} for the $^3H_4^{(1)} \rightarrow {}^3P_0$ excitation transition of Pr^{3+} and the $^6P_{7/2} \rightarrow {}^8S_{7/2}$ emission transition of Gd^{3+} in the same lattices, at 4.2 K.

	Gd^{3+} [a]		Pr^{3+} [b]	
Lattice	A_{VIB} (s^{-1})	A_{ZP} (s^{-1})	A_{VIB} (s^{-1})	A_{ZP} (s^{-1})
LaF_3	2	122	85	60
$LiYF_4$	6	122	100	840
La_2O_3	63	450	1600	2300

[a] After [1].
[b] This work.

Tables 2 and 3 show that A_{VIB} varies by nearly two orders of magnitude for both Gd^{3+} and Pr^{3+} ions. The vibronic coupling is much stronger for Pr^{3+} than for Gd^{3+}. These points will be discussed later.

Up till now, only vibronic transitions belonging to the Pr^{3+} $^3H_4^{(1)} \rightarrow {}^3P_0$ excitation transition were discussed. We will now consider the other intraconfigurational excitation transitions of Pr^{3+} (see figure 1).

Due to the large number of electronic lines, the $^3H_4^{(1)} \rightarrow {}^3P_1, {}^1I_6$ region is too complicated to study vibronics at all. The $^3H_4^{(1)} \rightarrow {}^3P_2$ transition consists of several electronic lines, since $J = 2$ for the final level. However, the crystal field splitting is usually small (about 200 cm^{-1}), and higher electronic levels are absent until the $^1S_0$ level at about 48 000 cm^{-1}. Consequently, this transition is suitable to observe vibronic lines due to coupling with high-frequency vibrations. This fact led to additional information only in $Y_3Al_5O_{12}$:Pr, where vibronic lines were observed at about 450 and 850 cm^{-1} from the most intense $^3H_4^{(1)} \rightarrow {}^3P_2$ zero-phonon line. The vibrational frequencies of all the other investigated compositions are lower than 500 cm^{-1}, and therefore most of the vibronics could be observed in the $^3H_4^{(1)} \rightarrow {}^3P_0$ region.

The relative position of the vibronics is the same for both excitation transitions, but in the $^3H_4^{(1)} \rightarrow {}^3P_2$ transition these positions cannot be unequivocally defined since several zero-phonon origins are present. For the same reason, the integrated intensity ratio R of the vibronic features and the zero-phonon lines carries a

considerable uncertainty for this transition. Nevertheless, the accuracy is high enough to show that the R-values of the $^3H_4^{(1)} \rightarrow {}^3P_2$ and $^3H_4^{(1)} \rightarrow {}^3P_0$ transitions are of the same order of magnitude and vary in the same way in different host lattices.

4. Theories on vibronic intensity in rare-earth spectra

There are several theoretical approaches to describe the intensity of vibronic transitions in rare-earth ions. Richardson and Faulkner [6] developed a general theory for vibronically induced electric-dipole intensities in f–f transitions. The model considers a RE^{3+} ion in octahedral coordination ($RECl_6$). The ligands interact through coulombic forces with the RE^{3+} ion giving rise to static and dynamic perturbations. Such perturbations are considered to be due to coupling of the 4f electronic term levels to the odd-parity part of the crystal-field potential (static term) and to the transient ligand dipoles induced by the *ungerade* vibrational modes (dynamic term). The model was applied to elpasolite systems $Cs_2NaRECl_6$ assuming coupling with the ν_3, ν_4 and ν_6 vibrational modes of the $RECl_6$ octahedron only. There is a good agreement between calculated and experimental vibronic oscillator strengths.

Judd [7] has worked out a similar approach to the same system using tensorial techniques. He has included in the static coupling the interaction between the 4f electrons and the dipole-field induced in the ligands by the net charge of the central metal ion. The dynamic coupling is extended to include the transient dipoles induced by the radiation field and the screening of the multipole fields by the outer electronic shells of the RE^{3+} ion.

Stavola *et al* [8] considered the possibility of cooperative vibronic transitions, i.e. a radiative transition involving a simultaneous electronic transition within the 4f shell and a vibrational transition of a nearby ligand molecule. Calculations are carried out based on an electrostatic two-centre coupling model applied to the RE^{3+}–OH system.

Later, Dexpert-Ghys and Auzel [9] observed vibronic lines in the absorption spectra of $Yb(OH,OD)_3$. These lines were attributed to cooperative transitions involving the Yb^{3+} ion and the O–H (O–D) stretching vibration. The authors showed that the cooperative model of Stavola [8] is equivalent to the static coupling models of Judd [7] or Richardson and Faulkner [6]. Further, they argued that the classical Franck–Condon replicas could also contribute to the vibronic intensity of ions in non-centrosymmetric sites. The contribution of Franck–Condon replicas to the intensity of f–f vibronic transitions is usually not considered, since the Huang–Rhys coupling factor S is assumed to be negligibly small for transitions within the 4f shell. However, the observed vibronic oscillator strengths in the Yb^{3+}–OH system could be accounted for by considering the transitions as Franck–Condon replicas with a Huang–Rhys factor of 10^{-2}. Therefore, neglecting the Franck–Condon principle is not justified.

The general outcome of these approaches is that the total vibronic transition probability is given by the summation of two contributions:

$$A_{VIB} = A_{VIB}((U^{(2)})) + A_{VIB}((U^{(\lambda)})) \tag{4}$$

where $A_{VIB}((U^{(2)}))$ gives the contribution of vibronically induced forced electric dipole transitions and $A_{VIB}((U^{(\lambda)}))$ gives the contribution due to the classical phonon replicas, i.e. transitions induced by a shift in the equilibrium position of the lattice configurational coordinates. The two processes are sometimes called M- and Δ-processes, respectively [31].

The vibronic oscillator strength due to the M-process, $P_{VIB}((U^{(2)}))$, can be described as follows [7]

$$P_{VIB}((U^{(2)})) = \chi 8\pi^2 \frac{m_e}{3h} \nu \frac{(U^{(2)})^2}{(2J+1)} (T^{(1)})^2 [P_{ST} + P_D] \tag{5}$$

where

$$P_{ST} = \tfrac{10}{3} e^4 R_L^{-6} N (g + N\alpha R_L^{-3})^2 \Xi_{(1,2)}^2 \tag{6}$$

and

$$P_D = 470(1-\sigma_2)^2 \alpha^2 R_L^{-10} \langle r^2 \rangle_{4f^n}^2 \tag{7}$$

where P_{ST} and P_D are the static and dynamic terms, ν is the frequency of the zero-phonon transition, N the coordination number of the RE ion, g and α the charge and polarizability of the ligand L, R_L the RE–L distance and χ the local-field correction term. $\Xi_{(1,2)}$ describes the first multipolar term (dipole–dipole) of the opposite-parity mixing. $(U^{(2)})$ is the reduced matrix element of the unit tensor operator $(U^{(\lambda)})$ connecting the electronic states. This matrix element imposes a selection rule on the vibronic transitions, viz. $\Delta J \leqslant 2$. The reduced matrix element $(T^{(1)})$ is equivalent to $|\langle 0\|T^{(1)}\|p\rangle|$, where the electric dipole (ED) operator $T^{(1)}$ links the initial vibrational state $|0\rangle$ to the final vibrational state $|p\rangle$. This matrix element predicts the most intense vibronic lines for coupling to IR-active vibrational modes. The term $\langle r^2 \rangle_{4f^n}$ in equation (7) is the average electron–nucleus distance and the parameter σ_2 accounts for the screening of the multipole field by the outer shells $5s^2$ and $5p^6$.

The contribution of the Δ-process to the vibronic oscillator strength can be expressed as [9, 26]

$$P_{VIB}((U^{(\lambda)})) = P_{ZP}((U^{(\lambda)}))S \qquad \lambda = 2,4,6 \tag{8}$$

where S is the Huang–Rhys coupling factor, which can be $10^{-2} - 10^{-1}$ for rare-earth(III) ions in solids [9].

5. Discussion

Table 2 shows that the vibronic transition probability A_{VIB} of the $^3H_4^{(1)} \rightarrow {}^3P_0$ transition of Pr^{3+} varies by two orders of magnitude with the host lattice. We shall now discuss the extent to which this variation can be accounted for by the theoretical approaches.

Vibronic transitions were observed for both the $^3H_4^{(1)} \rightarrow {}^3P_0$ ($\Delta J = 4$) and the $^3H_4^{(1)} \rightarrow {}^3P_2$ ($\Delta J = 2$) excitation transition of the Pr^{3+} ion. The magnitude of the ratio R between the total vibronic and electronic integrated intensities is similar for both transitions. This is a clear violation of the $\Delta J \leqslant 2$ selection rule for the M-process. In addition, the vibronic part of the spectra can be ascribed to coupling with IR- and Raman-active vibrational modes. The intensity of the vibronic lines does not appear to be determined by the Raman- or IR-active character of the phonons which couple to the electronic transition. This fact violates the selection rule which arises

from the ED operator $T^{(1)}$. Richardson *et al* [32, 33] have observed similar violations in the optical spectra of Pr^{3+} in Cs_2NaYCl_6 (elpasolite), where vibronic lines in purely magnetic dipole (MD) transitions as well as in the $^3H_4 \rightarrow {}^3P_0$ transition, and coupling to IR-inactive vibrational modes were found to take place. These violations have also been observed for Gd^{3+} (in, for example, YOCl [1], $Cs_2NaGdCl_6$ [1], Ba_2LaTaO_6 [34]) and Eu^{3+} [3].

These observations suggest that the main contribution to the vibronic intensity in the Pr^{3+} excitation transitions originates in the Δ-process.

The Δ-process contribution is defined by equation (8). The vibronic oscillator strength is related to the zero-phonon oscillator strength via the Huang–Rhys coupling parameter S. Therefore, (8) implies that A_{VIB} increases by increasing A_{ZP} or S, or both. Indeed, A_{ZP} increases from 60 s^{-1} in LaF_3 to 1.4×10^4 s^{-1} in Y_2O_2S. This variation leads to a factor of 200 in A_{VIB}. However, it should be considered that the value of A_{ZP} for the $^3H_4^{(1)} \rightarrow {}^3P_0$ transition of Pr^{3+} in LaF_3 is one order of magnitude smaller than that of Pr^{3+} in $LiYF_4$. The value of A_{ZP} for the $^3H_4^{(2)} \rightarrow {}^3P_0$ transition is 1600 s^{-1} for $LiYF_4$:Pr and 1700 s^{-1} for LaF_3:Pr. This fact may imply that the $^3H_4^{(1)} \rightarrow {}^3P_0$ transition probability of Pr^{3+} in LaF_3 is anomalously low and cannot be reliably compared to the A_{ZP} values for the other compositions. Comparing the value of A_{ZP} for $LiYF_4$:Pr^{3+} to that of Y_2O_2S:Pr^{3+}, a variation by a factor of 17 is found.

The Huang–Rhys parameter S can be derived from the expression $I_{ZP} = I_0 e^{-S}$, where I_{ZP} is the intensity of the zero-phonon line and I_0 is the total intensity. To estimate S we consider the vibronic lines at 155 cm^{-1} for $LiYF_4$:Pr (figure 2) and at 158 cm^{-1} (figure 3) for Y_2O_2S:Pr. These lines were chosen because they are the most intense lines which can be attributed to vibronic coupling with Raman-active vibrational modes. From their relative intensities we can derive S to be 0.02 for $LiYF_4$:Pr and 0.2 for Y_2O_2S:Pr. Taking the variation of A_{ZP} and S together, we have an increase of two orders of magnitude in A_{VIB} going from $LiYF_4$ to Y_2O_2S.

It can be observed from table 2 that the increase of A_{VIB} and A_{ZP} follows the shift to lower energies of the zero-phonon transition, of the 4f5d configuration and of the optical absorption edge of the lattice. These shifts can be ascribed to an increasing covalency. The increase in covalency can be considered as an increase of the spatial extension of the electronic wavefunctions of the metal ion and ligands. The larger extension of the 4f and ligand orbitals enhances the electron–phonon coupling strength and, consequently, the Huang–Rhys parameter S increases [35].

The zero-phonon transition probability A_{ZP} of the $^3H_4^{(1)} \rightarrow {}^3P_0$ transition has only an electric-dipole contribution [33]. The electric-dipole transition probability A_{ZP}^{ED} is expressed in terms of the Judd–Ofelt theory [36, 37]. The value of A_{ZP}^{ED} is proportional to the matrix elements $U^{(\lambda)}$ and to the Judd–Ofelt parameters Ω_λ, with $\lambda = 2, 4, 6$. Considering one particular transition, the $U^{(\lambda)}$-values do not vary with the host lattice. The phenomenological parameters Ω_λ are directly proportional to the strength of the odd-parity crystal-field terms and to the opposite-parity configuration admixing. The latter is given by the term $\Xi_{(t,\lambda)}$. The first multipolar term (dipole–dipole) of parity mixing, $t = 1$ and $\lambda = 2$, is defined by Judd [36] as a summation over all excited configurations. The admixture of opposite parity states is inversely proportional to $\Delta E_{(4f)(n'l')}$, the energy difference between the $4f^2$ and the excited $(n'l')$ configurations. Consequently, the shift of the first opposite-parity configuration 4f5d to lower energies increases the opposite-parity mixing, causing A_{ZP} to become larger.

In conclusion, the variation of two orders of magnitude in A_{VIB} can be accounted for within the framework of the Δ-process. The variation can be ascribed to the simultaneous increase of S and A_{ZP}, as a result of the increase in covalency and opposite-parity configuration admixing from top to bottom in table 2.

However, one should be cautious in claiming that only the Δ-process is operative. It should be kept in mind that the equations describing the M-process contribution (equations (5)–(7)) were derived for an isolated $RECl_6^{3-}$ complex and that only second-order perturbation terms were included [6, 7]. These assumptions allow a great simplification, but they may be a shortcoming to the theory.

The situation is similar to the violation of the $\Delta J \leqslant 2$ selection rule observed in two-photon absorption (TPA). Downer *et al* [38] have shown that the $\Delta J \leqslant 2$ selection rule, arising from second-order perturbation calculations, is lifted when higher-order (third or fourth) perturbation terms acting on the intermediate configurations are included. The contribution of the higher-order terms was shown to be large. The theory can account quantitatively for the observed TPA line strengths of $\Delta J = 0$, 2, 4 or 6 transitions and it was later extended to the spin-forbidden transitions of Gd^{3+} and Eu^{3+} [39]. Higher-order terms are expected to become more important as covalency increases.

We will now consider how far the observed variation on A_{VIB} can be accounted for by the M-process, if the $\Delta J \leqslant 2$ selection rule is lifted. The way in which A_{VIB} varies with the host lattice will be assumed to be the same as derived for $\Delta J \leqslant 2$. The increase in A_{VIB} follows the increase in the opposite-parity configuration mixing, given by the term $\Xi_{(1,2)}$, and the increase of covalency. Moreover, the optical absorption frequency of the lattice decreases from 80 000 cm^{-1} in LaF_3 to 41 000 cm^{-1} in Y_2O_2S (see table 2). This can be correlated to the increase of the polarizability α by using the formula

$$\alpha = \frac{e^2}{m}\sum_j \frac{f_{ij}}{(\nu_{ij}^2 - \nu^2)} \tag{9}$$

where ν is the frequency of the zero-phonon transition, ν_{ij} the absorption frequency of the transition $i \rightarrow j$, i.e. the host lattice absorption, and f_{ij} the corresponding oscillator strength [40]. The oscillator strengths of the lattice absorption transition will be different for lattices with F^-, O^{2-} or S^{2-} as anions, but values of f_{ij} are not available. Therefore, f_{ij} is taken constant in (9) and α is calculated to increase by a factor of 5 from LaF_3 to Y_2O_2S.

The polarizability α depends also on the specific surroundings of the anion [41]. The polarizability of the O^{2-} ion, for instance, has been found to be inversely proportional to the twelfth power of the anion–cation distance (R_L) in anisotropic surroundings, and to its third power in isotropic surroundings [42].

The magnitude of these effects is difficult to evaluate precisely, since the polarizability α of the anions in the lattices investigated are not known. For simplicity, an estimation will be performed by taking only the calculated frequency dependence into account: $\alpha_{Y_2O_2S} \sim 5\alpha_{LaF_3}$. This yields an increase by a factor of 25 in A_{VIB}, since α appears squared in equations (6) and (7).

The parameter $\Xi_{(1,2)}$ affects only the static coupling term P_{ST}. The lowest level of the 4f5d configuration decreases from 60 000 cm^{-1} in LaF_3 to 33 000 cm^{-1} in Y_2O_2S. This yields an increase by a factor of about 2 in $\Xi_{(1,2)}$, since this parameter is inversely proportional to $\Delta E_{(4f5d)}$ [36]. The value of A_{VIB} is expected to increase

by a factor of about 4, because the term $\Xi_{(1,2)}$ appears squared in (6). The variations of $\Xi_{(1,2)}$ and α taken together in (6) yield a factor of about 100 in A_{VIB}.

The covalency acts only on the dynamic coupling contribution via the terms $(1-\sigma_2)$ and $\langle r^2\rangle_f$ of (7). The parameter σ_2 is directly proportional to the screening of the 4f electrons by the outer shells $5s^2$ and $5p^6$. Increasing covalency leads to a larger overlap between the ligand and the 4f orbitals and the shielding will be substantially reduced. Simultaneously, the average electron–nucleus distance $\langle r^2\rangle_{4f^n}$ increases because of the the partial donation of electronic density from the ligands [7, 43, 44]. Consequently, the dynamic coupling contribution becomes larger as covalency increases [7]. However, the relationship between covalency and the parameters σ_2 and $\langle r^2\rangle_{4f^n}$ is very hard to quantify. Despite this, it is clear that an increase in covalency will increase A_{VIB}. The remaining parameters in equations (5)–(7) do not vary significantly with the host lattice.

In spite of the violation of the selection rules, it turns out from the preceding discussion that the observed variation of A_{VIB} can also be accounted for by assuming coupling due to the M-process, if we assume that the $\Delta J \leqslant 2$ selection rule is lifted.

Let us now consider table 3. It shows that the vibronic transition probabilities are 20 to 40 times larger in Pr^{3+} than in Gd^{3+} in the three host lattices. In spite of the differences concerning the matrix elements $U^{(\lambda)}$, the two ions can be usefully compared. For the $^3H_4 \rightarrow {}^3P_0$ transition on Pr^{3+} only $U^{(4)}$ is non-zero [45]. For the $^6P_{7/2} \rightarrow {}^8S_{7/2}$ transition on Gd^{3+} we have $U^{(2)} \gg U^{(4)} > U^{(6)}$ [46].

The value of A_{ZP} is larger for Pr^{3+} than for Gd^{3+}, since the matrix element $U^{(4)}$ of the $^3H_4 \rightarrow {}^3P_0$ transition on Pr^{3+} is larger than the matrix element $U^{(2)}$ of the $^6P_{7/2} \rightarrow {}^8S_{7/2}$ transition on Gd^{3+}, (0.414 [45] and 0.034 [46] respectively). Additionally, the opposite-parity states in Pr^{3+} are at lower energies than in Gd^{3+}, leading also to larger values of A_{ZP} because the term $\Xi_{(1,2)}$ increases [36]. As an example, we compare the values of $\Xi_{(1,2)}$ for Gd^{3+} in LaF_3 [1], 0.877×10^{-6} cm^2 erg^{-1}, and for free ion Pr^{3+} [47], 1.78×10^{-6} cm^2 erg^{-1}. In this connection we note that the increase of A_{VIB} with the lower position of the opposite-parity states has been explicitly shown by comparing the isoelectronic ($4f^7$) ions Gd^{3+} and Eu^{2+} in isostructural lattices YOCl and MFCl (M = Sr, Ba), respectively [2].

Moreover, the average electron–nucleus distance $\langle r^2\rangle_{4f^n}$ has been calculated as $1.09a_0^2$ for the $4f^2$ wavefunction of Pr^{3+} and $0.785a_0^2$ for the $4f^7$ wavefunction of Gd^{3+} [48]. This fact implies that the degree of covalency is higher for the Pr–ligand interaction. Indeed, the shift of the position of the electronic term levels with the host lattice is larger for the $^3P_0$ level of Pr^{3+} than for the $^6P_{7/2}$ level of Gd^{3+}. The $^3P_0$ level of Pr^{3+} shifts from 20 939 cm^{-1} in LaF_3 to 19 889 cm^{-1} in Y_2O_2S (table 2), whereas the $^6P_{7/2}$ level of Gd^{3+} shifts from 32 188 cm^{-1} to 31 720 cm^{-1} in the same host lattices [1, 49]. Because of the higher covalency, the Huang–Rhys parameter S is expected to be larger for Pr^{3+} than for Gd^{3+}. Therefore, the vibronic coupling strength due to the Δ-process is larger for Pr^{3+} than for Gd^{3+}, since the former ion has larger values of S and A_{ZP}.

In the previous discussion, we pointed out that the matrix element $U^{(4)}_{Pr}$ is larger than the matrix element $U^{(2)}_{Gd}$, and the parameters $\Xi_{(1,2)}$ and $\langle r^2\rangle_{4f^n}$ are larger for Pr^{3+} than for Gd^{3+}. The shielding coefficient σ_2 is smaller for the Pr^{3+} free ion [43] than for the Gd^{3+} free ion [44], (0.67 and 0.9, respectively). These parameters enter the equations describing the M-process (equations (5)–(7)). Consequently, the

vibronic coupling due to the M-process can be stronger for Pr^{3+} than for Gd^{3+}, if the $\Delta J \leqslant 2$ selection rule is lifted.

Therefore, we may conclude that the differences between the vibronic coupling strengths of Pr^{3+} and Gd^{3+} are due to the more extended 4f wavefunctions, the less effective 4f shielding, and the larger opposite-parity mixing in the case of the former ion.

6. Conclusions

Vibronic features are observed for the $^3H_4^{(1)} \rightarrow {}^3P_2$ and $^3H_4^{(1)} \rightarrow {}^3P_0$ excitation transitions of Pr^{3+} in several host lattices. The integrated intensity ratio R of the vibronic and zero-phonon lines are of the same order of magnitude for both transitions.

The vibronic transition probabilities for the $^3H_4^{(1)} \rightarrow {}^3P_0$ transition on Pr^{3+} vary by two orders of magnitude from LaF_3 to Y_2O_2S. This variation can be accounted for by assuming the Δ-process and considering the increase in the zero-phonon transition probability A_{ZP}, and in the Huang–Rhys parameter S. The variation of A_{ZP} and S can be correlated to the increase in the opposite-parity configuration admixing and in covalency, respectively. The host-lattice dependence of A_{VIB} can also be accounted for by considering coupling due to the M-process, if we assume that the $\Delta J \leqslant 2$ selection rule is lifted. In such a case the increase in the values of A_{VIB} can be attributed to an increase of the polarizability of the ligands, of the opposite-parity configuration admixing and of covalency.

The vibronic coupling is much stronger in Pr^{3+} than in Gd^{3+}. This fact is attributed to the more extended 4f orbitals, the larger opposite-parity mixing and the less effective shielding of the 4f electrons by the outer shells in the former ion.

Further investigations on the mechanisms involved in the Pr^{3+} vibronic interactions are in progress.

Acknowledgments

We wish to thank Dr D J Stufkens and Mr T Snoeck (University of Amsterdam) for measuring the Raman spectra of RE_2O_2S and La_2O_3, and Dr E B Stucchi (UNESP, São Paulo, Brazil) for measuring the IR absorption spectra of RE_2O_2S. One of us (CMD) wishes to thank the University of Utrecht for a temporary appointment and the CNPq (Conselho Nacional de Desenvolvimento Científico e Tecnológico, Brazil) for a study grant.

References

[1] Sytsma J, van Schaik W and Blasse G 1991 *J. Phys. Chem. Solids* **52** 419
[2] Sytsma J and Blasse G 1992 *J. Lumin.* **51** 283
[3] Blasse G 1990 *Inorg. Chim. Acta* **167** 33
[4] de Mello Donegá C and Blasse G 1991 *Chem. Phys. Lett.* **183** 367
[5] Blasse G 1992 *Int. Rev. Phys. Chem.* **11** 71
[6] Faulkner T R and Richardson F S 1978 *Mol. Phys.* **35** 1141
[7] Judd B R 1980 *Phys. Scr.* **21** 543

[8] Stavola M, Isganitis L and Sceats M G 1981 *J. Chem. Phys.* **74** 4228
[9] Dexpert-Ghys J and Auzel F 1984 *J. Chem. Phys.* **80** 4003
[10] Thoma R E, Weaver C F, Friedman H A, Insley H, Harris L A and Yakel H A 1961 *J. Phys. Chem.* **65** 1096
[11] Zalkin A, Templeton D H and Hopkins T E 1966 *Inorg. Chem.* **5** 1466
[12] Wyckoff W G 1961 *Crystal Structures* vol II (New York: Wiley)
[13] Templeton D H and Dauben C H 1953 *J. Am. Chem. Soc.* **75** 6069
[14] Gopinath C R and Brown I D 1982 *J. Raman Spectrosc.* **12** 278
[15] Carnall W T, Crosswhite H and Crosswhite H M 1977 Energy level structure and transition probabilities of the trivalent lanthanides in LaF_3 *Argonne Natl Laboratory Report*
[16] Hurrel J P, Porto S P S, Chang I F, Mitra S S and Bauman R P 1968 *Phys. Rev.* **173** 851
[17] Miller S A, Rast H E and Caspers H H 1970 *J. Chem. Phys.* **52** 4172
[18] Hoshina T, Imanaga S and Yokono S 1977 *J. Lumin.* **15** 455
[19] Yen W M, Scott W C and Schawlow A L 1964 *Phys. Rev.* A **136** 271
[20] Sytsma J and Blasse G 1992 *J. Phys. Chem. Solids* **53** 561
[21] Rast H E, Caspers H H and Miller S A 1968 *Phys. Rev.* **171** 1051
[22] Cerdeira F, Lemos V and Katiyar R S 1979 *Phys. Rev.* B **19** 5413
[23] Tolbert W A, Dennis W M and Yen W M 1990 *Phys. Rev. Lett.* **65** 607
[24] Rulmont A 1972 *Spectrochim. Acta* A **28** 1287
[25] Haeuseler H 1984 *J. Raman Spectrosc.* **15** 120
[26] Henderson B and Imbusch G F 1989 *Optical Spectroscopy of Inorganic Solids* (Oxford: Oxford University Press)
[27] Elias L R, Heaps Wm S and Yen W M 1973 *Phys. Rev.* B **8** 4989
[28] Ropp R C 1964 *J. Electrochem. Soc.* **111** 311
[29] Szczurek T and Schlesinger M 1985 *Rare-Earth Spectroscopy* ed B Jezowska-Trezbiatowska, J Legendziewick and S Stręk (Singapore: World Scientific) p 325
[30] Meilman M L, Kolomiitsev A I, Kevorkov A M and Bagdasarov Kh S 1984 *Opt. Spectrosc.* **57** 145
[31] Miyakawa T 1973 *Luminescence of Crystals, Molecules and Solutions* ed F Williams (New York: Plenum) p 394
[32] Richardson F S, Reid M F, Dallara J J and Smith R D 1985 *J. Chem. Phys.* **83** 3813
[33] Morley J P, Faulkner T R, Richardson F S and Schwartz R W 1982 *J. Chem. Phys.* **77** 1734
[34] Blasse G and Brixner L H 1990 *Inorg. Chim. Acta* **169** 25
[35] Auzel F 1991 *Advances in Non Radiative Processes in Solids* ed B Di Bartolo (New York: Plenum) p 164
[36] Judd B R 1962 *Phys. Rev.* **127** 750
[37] Ofelt G S 1962 *J. Chem. Phys.* **37** 339
[38] Downer M C 1989 *Laser Spectroscopy of Solids II* ed W M Yen (Heidelberg: Springer) ch 2
[39] Downer M C, Burdick G W and Sardar D K 1988 *J. Chem. Phys.* **89** 1787
[40] Kittel C 1976 *Introduction to Solid State Physics* (New York: Wiley)
[41] Bilz H, Büttner H, Bussman-Holder A and Vogl P 1987 *Ferroelectrics* **73** 493
[42] Bussmann A, Bilz H, Roenpiess R and Schwartz K 1980 *Ferroelectrics* **25** 343
[43] Sternheimer R M, Blume M and Peierls R F 1968 *Phys. Rev.* **173** 376
[44] Newman D J and Price D C 1975 *J. Phys. C: Solid State Phys.* **8** 2985
[45] Weber M J 1968 *J. Chem. Phys.* **48** 4774
[46] Detrio J A 1971 *Phys. Rev.* B **4** 1422
[47] Krupke W F 1966 *Phys. Rev.* B **145** 325
[48] Freeman A J and Watson R E 1962 *Phys. Rev.* **127** 2058
[49] Blasse G, Brixner L H and Hyatt G 1989 *Chem. Phys. Lett.* **164** 617